Modeling of Bubble-Size Distribution in Free Rise Polyurethane Foams

Debdarsan Niyogi, R. Kumar, and K. S. Gandhi
Dept. of Chemical Engineering, Indian Institute of Science, Bangalore-560 012, India

The existing models of the foaming process in reaction injection molding are inadequate for predicting the bubble-size distribution, which influences many properties of interest. This work attempts to develop a model for the bubble-size distribution under conditions of free rise.

The population balance equation for bubbles, coupled with the system of energy balance and reaction kinetics equations through the blowing agent evaporation rate expression, is solved to obtain the bubble-size distribution. A simple mass-transfer coefficient approach for expressing growth rate of bubbles is used, although various growth laws can be accommodated without affecting the solution procedure. Determining factors for the bubble size and its distribution are the foaming period and the growth law. With increase in initial blowing agent concentration, the foaming period increases and bigger bubbles are obtained. The bubble-size distribution becomes broader as the foaming period increases.

Introduction

Foamed polyurethanes are produced often by reaction injection molding (RIM). In this process, a mixture of polyol, isocyanate, catalyst and blowing agent is injected into a mold. The temperature of the reaction mixture rises due to the exothermicity of the polymerization reaction between polyol and isocyanate. Consequently, the mixture becomes supersaturated with respect to the blowing agent, and nucleation of bubbles occurs. And then, formation of new bubbles due to nucleation and growth of already nucleated bubbles occur simultaneously and continuously. Both processes are usually halted due to the formation of a cross-linked gel. As the age of bubbles and their growth histories are not identical, they will not be of equal size in the final cross-linked product.

Many models of the foaming process under free rising conditions (open molds) (Rojas et al., 1982; Marciano et al., 1986), as well as when integral-skin foams are obtained (closed molds) (Yokono et al., 1986; Tighe et al., 1988), have been reported. The models for integral-skin foams assume that foam rises at atmospheric pressure in the closed mold, until the mold is completely filled. Up to this point, models for both open and closed molds will be similar. Campbell (1972a,b) was the first to develop a computer simulation for skin formation in a closed-mold cavity. The main drawbacks of his model are: the arbitrary definition of the fraction of heat used for vaporization of the blowing agent, the assumption that boiling temperature is independent of concentration of blowing agent and is a sole function of pressure, neglect of onset of gelation, and the assumption of complete evaporation of the blowing agent. Rojas et al. (1982) proposed a model for free rising rigid polyurethane foams based on more realistic assumptions. In this model, adiabatic conditions are assumed. Reaction kinetics and the relationship between the liquid-phase blowing agent concentration and the boiling temperature are obtained experimentally. Simulation is carried out up to the gel point. It is assumed, however, that the temperature of the solution is always equal to the boiling point corresponding to the blowing agent concentration in the solution. Three quantities of interest to be predicted by a model are the cream time, rise time, and foam density. The time required for the blowing agent to nucleate and vaporize is called cream time, and rise time, in open mold or free rise case, is defined as the period in which a sufficient rigidity of the reaction mixture is reached due to gelatin and rising stops. The model developed by Rojas et al. (1982) predicts these three quantities as a function of the initial concentration of the blowing agent. The simulated results compared favorably with the experimental ones.

The models that assume thermodynamic equilibrium be-

Correspondence concerning this article should be addressed to R. Kumar.

tween vapor and liquid phases, such as those discussed above, cannot predict the bubble-size distribution in the foams since nucleation and bubble growth phenomena have been ignored. The physico-mechanical properties such as elasticity and strength, as well as the thermophysical properties such as thermal conductivity, are influenced strongly by the bubble-size distribution (Shutov, 1983). In this work, attention is focused on the prediction of the bubble-size distribution generated during free rise foaming.

Foaming of thermoplastics by solvents is similar to that of polyurethanes as far as bubble nucleation and growth are concerned. Amon and Denson (1984) have developed a cell model for bubble growth in thermoplastics under isothermal and isobaric conditions, when the mass of the blowing agent is negligible compared to that of the polymer. Under these conditions, the bubbles cannot grow beyond a certain equilibrium size. Their results for bubble growth under diffusion-controlled conditions suggest that the growth rates decay to zero toward the end stages of expansion as the bubbles approach their equilibrium sizes. Prior to that, their results suggest that the increase in the radius of the bubble is approximately proportional to the square root of the time. Amon and Denson (1986) have also integrated this bubble growth model into a model of low-pressure structural foam molding of a thermoplastic. In this process, a short shot of supersaturated thermoplastic is injected into a cold mold. The thermoplastic freezes progressively inward from the mold walls as it rises, and bubbles can grow only in the molten zone. Thus, the mold consists of a zone where bubbles grow and another where they cannot, and it is this nonhomogeneity that produces a bubble-size distribution in the sample. In this sense, the source of nonuniformity in bubble-size distribution here differs from that in reaction injection-molded polyurethane foams, and we will discuss this aspect in greater detail later.

The classical theory of homogeneous nucleation suggests that the rate of nucleation depends on the free energy change due to the formation of a nucleus of the critical size. Han and Han (1990a,b) have reviewed the literature on homogeneous nucleation in polymer solutions. They suggest that the nonideal nature of polymer solutions and the extent of supersaturation have to be incorporated directly into the classical theory of homogeneous nucleation to account for the rate of nucleation in polymer solutions and have presented an expression to compute it based on their experimental data. In real systems, it is possible that nucleation may be heterogeneous in character due to the presence of solid particles. The rate of heterogeneous nucleation is faster than that of homogeneous nucleation, but no general theory exists to compute it. Hence, we develop a theory based on homogeneous nucleation, but will present a qualitative assessment of the implications of these aspects during the discussion of our results.

Physical System and Assumptions

The model deals with solvent-blown RIM and is suitable for describing free rising foams. The mold is partially filled with the reactive-mixture-containing polyol, isocyanate, blowing agent, and small amounts of catalyst and surfactant. Exothermic polymerization reaction takes place between polyol and isocyanate, thereby raising the temperature of the mixture. As the temperature exceeds the boiling point of the reaction mixture, nuclei are formed. These nuclei grow to bubbles by vaporization of the liquid phase, and the mixture foams and rises. Bubbles also increase in volume due to an increase in temperature. Supersaturation is not consumed immediately after the first nucleating events, and thus growth and nucleation occur simultaneously for some time. This gives rise to a bubble-size distribution.

The assumptions made in the development of this model are:

1. The mold is assumed to be a cylindrical cup of uniform cross-section to facilitate comparison with the results of Rojas et al. (1982).
2. In this work, we do not consider growth of bubbles in the soft elastic gel. Thus, we assume that bubble growth and nucleation come to a halt as soon as the gel point is reached.
3. The nucleation is assumed to be homogeneous.
4. Adiabatic conditions are assumed. This implies that all conditions, including the bubble nucleation, are spatially uniform and that the gelation occurs at the same instant throughout the mold. Hence, bubble growth comes to a halt in the entire mold at the same time. This is to be contrasted with the nonhomogeneity of growth conditions prevailing in the thermoplastic foam molding considered by Amon and Denson (1986).
5. We assume that the bubbles do not coalesce due to the presence of surfactants.
6. Liquid-to-gas mass transfer is considered to be purely diffusional and controlled by the liquid-side resistance. Bubble growth in viscoelastic media is a very complex phenomenon. In this work, three simple mass-transfer coefficient models have been assumed for making predictions. The solution procedure, however, remains independent of this assumption and can accommodate arbitrarily complex growth laws.
7. As polymerization progresses, viscosity increases and reaches a high value before the boiling point of the mixture is reached. Under these conditions, the relative motion between the bubbles and the liquid is negligible, and has hence been ignored.
8. The blowing agent was assumed to behave as an ideal gas in the vapor phase.
9. Because blowing agent is much more volatile than the polymer and monomers present in the solution, evaporation of the latter has been ignored.

In addition, the following assumptions made by previous workers have also been made:

10. Volume changes due to mixing in liquid phase have been neglected.
11. Physical properties like specific heats, heat of reaction, latent heat of vaporization and densities of liquid-phase components have been assumed to be constant within the temperature range of interest. We assume that density and specific heat of the polymer equal those of the monomer mixture.

Mathematical Formulation

The energy balance equation has to be solved together with the kinetics of the polymerization and blowing agent evaporation rate. A population balance equation has to be formulated to account for the bubble sizes. It is linked with the other system of equations through the rate of evaporation of blowing agent.

Energy balance

The prepolymer-blowing agent mixture gains heat due to the exothermic polymerization reaction and gives away heat for evaporation of the blowing agent. The unsteady heat balance equation for liquid and gas phases combined becomes:

$$\frac{d}{dt}\left[(m_p c_{p_p} + m_B c_{p_B})T\right] + \frac{d}{dt}\left[(m_{B0} - m_B)c_{p_g}T\right] = (-\Delta H_r)\frac{m_p}{IEW}\frac{dx}{dt} + \lambda\frac{dm_B}{dt} \quad (1)$$

In the above equation, both the gas- and liquid-phase specific heats are taken into account separately.

Polymerization reaction rate

The kinetics of urethane formation are complex and have been studied by the adiabatic temperature rise method. To facilitate comparison with the results of Rojas et al. (1982), we use the second-order kinetics proposed by Marciano et al. (1982). The usual form for a batch reactor is:

$$\frac{dx}{dt} = A\exp\left[-\frac{E}{RT}\right](1-x)^2 \quad (2)$$

The above kinetic expression has also been obtained by conducting adiabatic temperature rise studies up to gelation (Lipshitz et al., 1977; Marciano et al., 1982). But the formulation used by them did not contain a blowing agent. So, to account for the dilution caused by the presence of blowing agent, the above equation is modified as follows:

$$\frac{dx}{dt} = A\left[\frac{\rho_L}{\rho_p}(1-W_B)\right]\exp\left[-\frac{E}{RT}\right](1-x)^2 \quad (3)$$

The influence of the correction factor is negligible for low concentrations of the blowing agent (4% reduction in initial reaction rate for $W_{B_o} = 0.044$), but becomes significant when the blowing agent concentration is high (14% reduction in initial reaction rate for $W_{B_o} = 0.171$). ρ_L is obtained by the following relation:

$$\rho_L = \frac{1}{(1-W_B)/\rho_p + W_B/\rho_B} \quad (4)$$

Rate of blowing agent evaporation

Let $N(l)$ be the overall rate of evaporation into a bubble of size l. If the number density of bubbles per unit volume of liquid phase in size range between l and $l+dl$ is $f(l)dl$, the rate of decrease of mass of blowing agent in the bulk liquid is given by:

$$-\frac{dm_B}{dt} = -\frac{d}{dt}(V_L C_B M_B) = \int_{l_N}^{\infty} M_B[N(l)f(l)V_L]dl \quad (5)$$

Thus, it is clearly seen that bubble-size distribution is necessary to solve Eqs. 1-5. Rate of mass transfer into a bubble of diameter l can be expressed as:

$$N(l) = k_m \pi l^2 (C_B - C_B^*) = k_m \pi l^2 \Delta C_B \quad (6)$$

The gas bubble contains only blowing agent and the pressure (P) inside it is atmospheric. Marciano et al. (1986) presented data on freon-blown polyurethane foams. To compare model predictions with their data feasible, we use the equilibrium data presented by them. The equilibrium concentration of freon at boiling point, C_B^*, was determined from the experimental correlation of Marciano et al. (1986) between blowing agent weight fraction in the mixture and its normal boiling point:

$$W_B^* = \frac{0.314}{\exp\left[(2{,}980 - 10.034T)/(191.22 - T)\right] - 0.686} \quad (7)$$

Here, capillary pressure effects have been neglected, and W_B^* is taken to be the same for all bubbles. Thus, errors occur only for very small bubbles.

Nucleation rate

Han and Han (1990a,b) suggest the following expression for net free energy change for the formation of a critical nucleus (ΔF_p^*) in polymer solution:

$$\Delta F_p^* = \Delta F^* - \Delta F_S - \Delta F_t \quad (8)$$

where

$$\Delta F^* = \frac{16\pi\sigma^3}{3(P_V - P_L)^2} \quad (9)$$

$$\Delta F_S = nkT \ln\left[S(t)\right] = nkT \ln\left[\frac{C_B}{C_B^*}\right] \quad (10)$$

ΔF_t is the free energy change of solvent due to the presence of macromolecules in the polymeric solution. This is estimated from Flory-Huggins theory:

$$\Delta F_t = nkT\left[\ln(1-\Phi) + \Phi + \chi\Phi^2\right] \quad (11)$$

In our formulation, Φ was approximated by the weight fraction of polymer, and χ, the interaction parameter, was assumed to be 0.5. In this work, it was found that the contribution of ΔF_t to ΔF_p^* is not large. Hence, the value of χ does not affect the results significantly. The nucleation rate in polymer solution is given by:

$$J = M\,B\exp\left[\frac{-\Delta F_p^*}{nkT}\right] \quad (12)$$

The frequency factor B essentially signifies the frequency with which the blowing agent gas molecules impinge on the nucleus and is a complex function of molecular vibrational frequency, activation energy for diffusion in polymer, surface area of critical nucleus, and so on. Generally, the frequency factor B is considered as an adjustable parameter due to a lack of

experimental data for evaluating it correctly. The same procedure is followed here.

For evaluating ΔF^*, P_V, the vapor pressure exerted by the liquid phase is required. As the system is nonideal, the liquid-phase activity coefficient is needed to calculate the vapor pressure exerted by the liquid phase. Efforts to fit the normal boiling point data of Marciano et al. (1986) to the Flory-Huggins equation were unsuccessful. Thus, activity coefficients were defined based on weight fraction for simplicity:

$$\gamma_B W_B P^{\text{sat}}(T) = P_V \tag{13}$$

For the temperature range of interest, $P^{\text{sat}}(T)$ is evaluated by using the Antoine equation:

$$P^{\text{sat}}(T) = \exp\left[AntA - AntB/(T + AntC)\right] \tag{14}$$

The activity coefficients in the liquid phase were calculated from the normal boiling point data represented by Eq. 7:

$$\gamma_B W_B P^{\text{sat}}(T^*) = 1 \text{ atm} \tag{15}$$

The values of γ_B calculated as function of W_B were fitted into two polynomials suitable for two ranges of values of W_B.

Population balance equation

In the absence of breakage and coalescence, the population balance equation for bubbles of size between l and $(l+dl)$ is given by:

$$\frac{\partial}{\partial t}[fV_L] + \frac{\partial}{\partial l}[fGV_L] = 0 \tag{16}$$

The initial condition for the population balance equation may prescribe an arbitrary distribution:

$$t = 0, \quad f = f(0, l); \quad \text{all } l \tag{17}$$

The boundary condition for l will be specified at the critical nucleus size and is given by:

$$l = l_N, \quad fV_L(t, l_N) = \frac{J(t)V_L(t)}{G(l_N, t)}; \quad \text{all } t \tag{18}$$

The growth rate of a bubble of size l can be obtained from a mass-balance equation for a single bubble, assuming ideal behavior of the vapor phase:

$$\frac{d}{dt}\left[\frac{\pi}{6} l^3 \frac{P}{RT}\right] = N(l) = k_m \pi l^2 \Delta C_B$$

or

$$\frac{dl}{dt} = G = \frac{2k_m RT \Delta C_B}{P} + \frac{l}{3T}\frac{dT}{dt} \tag{19}$$

A formal solution to Eqs. 16-19 can be written to obtain the bubble size distribution and is discussed below.

Bubble-size distribution

Expanding and rearranging the population balance (Eq. 16) we obtain:

$$\frac{1}{fV_L}\frac{\partial}{\partial t}(fV_L) + \frac{G}{fV_L}\frac{\partial}{\partial l}(fV_L) = -\frac{\partial G}{\partial l} = -2\frac{RT}{P}\Delta C_B \frac{dk_m}{dl} - \frac{1}{3T}\frac{dT}{dt} \tag{20}$$

The method of characteristics can be used to obtain the solution of the above equation. The characteristics are defined by:

$$\frac{dt}{dZ} = 1 \tag{21}$$

$$\frac{dl}{dZ} = G \tag{22}$$

Under this transformation, Eq. 20 becomes,

$$\frac{d}{dZ}\ln\left(fV_L T^{1/3}\right) = -\frac{2RT}{P}\Delta C_B \frac{dk_m}{dl} \tag{23}$$

Integration of Eq. 21 gives,

$$t = Z + r \tag{24}$$

where r represents the time at the beginning of a particular characteristic. Thus, fV_L is now regarded as a function of Z and r. The boundary condition has to be specified at the starting point of all characteristics, at $l = l_N$, as shown in Figure 1. Integration of Eq. 22 relates l to Z and r as:

$$\int_{Z=0,\,r}^{Z,\,r} dl = l(Z, r) - l_N = \int_{Z=0,\,r}^{Z,\,r} G\, dZ = \int_{t'=r}^{t'=t}\left[\frac{2k_m RT}{P}\Delta C_B + \frac{1}{3T}\frac{dT}{dt}\right] dt' \tag{25}$$

where Eq. 24 has been used to replace Z. Now, Eq. 23 itself can be integrated using Eq. 24 to obtain:

$$\ln\left[\frac{fV_L T^{1/3}|_{Z,\,r}}{fV_L T^{1/3}|_{Z=0,\,r}}\right] = -\int_{t'=r}^{t'=t}\frac{2RT\Delta C_B}{P}\frac{dk_m}{dl}\,dt' \tag{26}$$

In the above $(fV_L)|_{Z=0,\,r}$ equals the value of fV_L at $l = l_N$ and time r, and can be obtained from Eq. 18. Once Z and r are specified, Eqs. 24-26 can be used to obtain fV_L as a function of l and t, and thus the above constitutes the formal solution to the population balance equation. Equations 24-26 have to be integrated numerically and simultaneously with Eqs. 1-6. Thus, after bubble nucleation begins at cream time, bubble-size distribution can be obtained if the above procedure is followed by starting characteristics at different points of time (for different values of r). The above process is shown in Figure 1. It may be noted that the above procedure can, in principle,

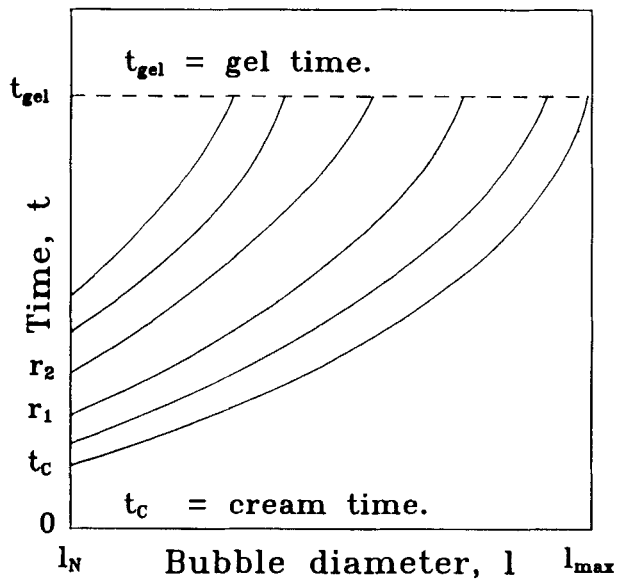

Figure 1. Characteristic curves on *t-l* plane.

accommodate any growth rate law in place of the mass-transfer coefficient model used.

With the help of the solutions obtained, properties of the foam can be calculated. The overall foam density is given by:

$$\rho_{all} = \frac{1}{(W_{B_o} - W_B)RT/(PM_B) + \dfrac{(1 - W_{B_o})}{\rho_p} + \dfrac{W_B}{\rho_B}} \tag{27}$$

Foam volume at any instant is obtained by:

$$V = V_L + \frac{\pi}{3} V_L \int_{l_N}^{\infty} l^3 f(l)\, dl \tag{28}$$

Moments of population balance equation

Moments of the population balance simplify the computations considerably as will be shown later. Thus, we derive equations for moments. The nth moment is obtained by multiplying the population balance equation by l^n and integrating over the range of sizes of bubble. Using the fact that $f(l)$ vanishes as $l \to \infty$, applying boundary condition (Eq. 18), and substituting for G from Eq. 19, the following equation is obtained:

$$\frac{1}{V_L}\frac{d(f_n V_L)}{dt} = l_N^n J(t) + n \int_{l_N}^{\infty} l^{n-1} \left[2k_m RT\,(C_B - C_B^*) + \frac{l}{3T}\frac{dT}{dt} \right] f\, dl \tag{29}$$

Mass-transfer coefficient

It is necessary to know the dependence of k_m to solve the above equations. If it is assumed that convection is negligible and mass transfer is diffusional and controlled by liquid-side resistance, Sherwood number can be taken to be 2 and diffusional mass-transfer coefficient k_D becomes:

$$k_D = \frac{2D}{l} \tag{30}$$

It may be mentioned here that D is assumed to be constant, the above expression predicts that the bubble radius will grow as the square root of time. This is consistent with the predictions of Amon and Denson (1984) for growth rates, except towards the final stages of growth.

The formulation also contains surfactant. The surfactant molecules accumulate at the gas-liquid interface and may offer an interfacial resistance. To incorporate the effect of surface resistance offered by surfactant, a series resistance model can be used and overall mass-transfer coefficient k_m can be written as:

$$k_m = \frac{k_D k_S}{k_S + k_D} = \frac{2Dk_S}{lk_S + 2D} \tag{31}$$

Now, the formulation is complete and computations can be made. If this overall coefficient k_m is used in Eq. 5, cumbersome expressions containing fractional moments are obtained. To illustrate the physical features, two limiting situations of purely diffusion-controlled and purely surface-resistance-controlled mass transfer are taken.

Solutions for Three Cases

Surface-resistance-controlled mass transfer

For this case,

$$k_m = k_S = \text{constant} \tag{32}$$

When this is incorporated into Eq. 5, the expression for blowing agent evaporation rate simplifies to:

$$-\frac{dm_B}{dt} = -\frac{d}{dt}(V_L C_B M_B) = \pi k_S \Delta C_B M_B \int_{l_N}^{l_{max}} l^2 f V_L\, dl = \pi k_S \Delta C_B M_B f_2 V_L \tag{33}$$

The growth rate of bubbles is obtained from Eq. 19:

$$G = \frac{2RTk_S \Delta C_B}{P} + \frac{l}{3T}\frac{dT}{dt} \tag{34}$$

The following equations for various moments are obtained by substituting k_S in place of k_m in Eq. 29 and integrating:

$$\frac{d(f_0 V_L)}{dt} = J(t) V_L(t) \tag{35}$$

$$\frac{d(f_1 V_L)}{dt} = \frac{2RTk_S \Delta C_B}{P} f_0 V_L + \frac{1}{3T}\frac{dT}{dt} f_1 V_L + l_N J(t) V_L(t) \tag{36}$$

$$\frac{d(f_2V_L)}{dt}=\frac{4RTk_S\Delta C_B}{P}f_1V_L+\frac{2}{3T}\frac{dT}{dt}f_2V_L+l_N^2J(t)V_L(t) \quad (37)$$

$$\frac{d(f_3V_L)}{dt}=\frac{6RTk_S\Delta C_B}{P}f_2V_L+\frac{1}{T}\frac{dT}{dt}f_3V_L+l_N^3J(t)V_L(t) \quad (38)$$

Equations 33–38 are self-contained and can be solved along with the equation for energy balance and reaction kinetics to obtain x, W_B, and T without obtaining the bubble-size distribution. This is a considerable simplification. The bubble-size distribution is obtained as follows. For this special case, Eq. 25 simplifies to:

$$l(Z,r)-l_N+\frac{1}{3}\ln\left[\frac{T(t)}{T(r)}\right]=\int_r^t\frac{2k_SRT\Delta C_B}{P}dt' \quad (39)$$

The righthand side of the Eq. 26 equals zero and hence,

$$\ln\left[(fV_L)\,|_{Z,r}T^{1/3}(t)\right]=\ln\left[(fV_L)\,|_{Z=0,r}T^{1/3}(r)\right] \quad (40)$$

The lefthand side for a particular characteristic curve started at time = r can be obtained by using the boundary condition (Eq. 18). Hence,

$$\ln\left[(fV_L)\,|_{Z=0,r}T^{1/3}(r)\right]=\ln\left[\frac{J(r)V_L(r)T^{1/3}(r)}{G|_{l_N}}\right] \quad (41)$$

The set of ordinary differential equations (Eqs. 1, 3, 33, 35–38) and the characteristic equations (Eqs. 39 and 40) are solved simultaneously to obtain the bubble-size distribution, as well as other properties of foam.

Diffusion-controlled mass-transfer (constant D)

For the case of purely diffusional mass transfer, mass-transfer coefficient k_m is given by:

$$k_m=\frac{2D}{l} \quad (42)$$

The diffusion coefficient D in this model is assumed to be constant. Using Eq. 42, the rate of depletion of mass of blowing agent is given by:

$$-\frac{dm_B}{dt}=-\frac{d}{dt}(V_LC_BM_B)=\pi k_m\Delta C_BM_B\int_{l_N}^{l_{\max}}lfV_Ldl$$

$$=2\pi D\Delta C_BM_Bf_1V_L \quad (43)$$

The growth rate is obtained from Eq. 19 by substituting k_m:

$$G=\frac{dl}{dt}=\frac{4RTD\Delta C_B}{Pl}+\frac{l}{3T}\frac{dT}{dt} \quad (44)$$

The following moment equations for various moments are obtained by substituting Eq. 44 in Eq. 27 and integrating:

$$\frac{d(f_0V_L)}{dt}=J(t)V_L(t) \quad (45)$$

$$\frac{d(f_2V_L)}{dt}=\frac{8RTD\Delta C_B}{P}f_0V_L+\frac{2}{3T}\frac{dT}{dt}f_2V_L+l_N^2J(t)V_L(t) \quad (46)$$

$$\frac{d(f_3V_L)}{dt}=\frac{12RTD\Delta C_B}{P}f_1V_L+\frac{1}{T}\frac{dT}{dt}f_3V_L+l_N^3J(t)V_L(t) \quad (47)$$

An expression for f_1V_L derived in a similar manner involves $f_{-1}V_L$, and $f_{-1}V_L$ will require $f_{-2}V_L$, and so the system of equations is never closed. For this case, it has to be evaluated only from its definition:

$$f_1V_L=\int_{l_N}^{\infty}lfV_Ldl \quad (48)$$

Thus, it is necessary to find the bubble-size distribution for this case, unlike the case just previously considered, to find x, W_B, T, and so on. This is achieved as follows. Equation 44 can be rewritten in terms of variables used to describe characteristics as:

$$\frac{d}{dt}(l^2T^{-2/3})=\frac{d(l^2T^{-2/3})}{dZ}=\frac{8RT^{1/3}D\Delta C_B}{P} \quad (49)$$

Initial condition for the above equation is:

$$\text{at } Z=0 \text{ or } t=r,\ \left(l_N^2T^{-\frac{2}{3}}\right)_{Z=0 \text{ or } t=r}=l_N^2T^{-\frac{2}{3}}(r) \quad (50)$$

Integrating,

$$l^2(Z,r)T^{-\frac{2}{3}}(t)-l_N^2T^{-\frac{2}{3}}(r)=\int_{t'=r}^{t'=t}\frac{8RT^{1/3}(t')D\Delta C_B(t')}{P}dt' \quad (51)$$

The righthand side integral can be evaluated and thus the diameter for the bubbles born at any time r is known as a function of time. The number density function fV_L as a function of bubble diameter and time can be obtained in the following way. Substituting k_m from Eq. 42 in Eq. 23 we get:

$$\frac{d[\ln(fV_LT^{1/3})]}{dZ}=\frac{4RTD\Delta C_B}{Pl^2} \quad (52)$$

Using Eq. 49, we get:

$$\frac{d[\ln(fV_LT^{1/3})]}{dZ}=\frac{d[\ln(lT^{-1/3})]}{dZ}$$

Integrating,

Table 1. Properties of the Reactants*

Reactant	Avg. Molecular Weight	Avg. Functionality
Polymethylenepolyphenyl Isocyanate (PAPI 135)	360.45	2.7
Polyetherpolyol Based on Sorbitol (NIAX LS 490)	550.0	4.8

*From Marciano et al. (1982).

$$\ln\left(\frac{fV_L T^{2/3}}{l}\right)\Bigg|_{Z,\,r} = \ln\left[\frac{(fV_L)|_{Z=0,\,r}T^{2/3}(r)}{l_N}\right] \tag{53}$$

The value of the righthand side for a particular characteristic curve started at time = r can be obtained as before by using the boundary condition (Eq. 18). Thus,

$$\ln\left[\frac{(fV_L)|_{Z,r}T^{2/3}(t)}{l(Z,\,r)}\right] = \ln\left[\frac{J(r)V_L(r)T^{1/3}(r)}{(Gl)|_{l_N}}\right] \tag{54}$$

A characteristic is defined by the value of r. Thus, once r is specified, we get the value of l from Eq. 51, for any t and use it to get corresponding fV_L value from the above equation. Thus, bubble-size distributions can be generated by using different values of $r < t$. Once bubble-size distribution is obtained, Eq. 48 can be used to obtain $f_1 V_L(t)$.

Hence, the set of ordinary differential equations (Eqs. 1, 3, 43, 45–48, 49 and 53) can be solved simultaneously to obtain the bubble-size distribution and other properties of foam.

Diffusion-controlled mass transfer (variable D)

Due to the chemo-rheological changes taking place, it can be expected that diffusion coefficient also changes. As polymerization reaction progresses, polymer molecular weight increases, and thus diffusion coefficient should decrease with time. We account for this change in D by assuming diffusion coefficient to be inversely proportional to the cube of molecular weight. The following equation can be written to account for this:

$$D = D_0(1-x)^3 \tag{55}$$

where x is the fractional conversion of isocyanate. The governing equations are the same as those for constant diffusion case; the only difference being the use of the Eq. 55 to evaluate the variation of diffusion coefficient with time.

Table 2. Physical Property Data

Property	Species	Symbol	Value	Unit
Density*	Polymer	ρ_p	1,160	kg/m^3
	Freon	ρ_B	1,467	"
Specific Heat*	Polymer	C_{p_p}	1,786.6	J/kg·K
	Freon (vap)	C_{p_g}	564.84	"
	Freon (liq)	C_{p_B}	920.48	"
Latent Heat of Vaporization*	Freon	λ	1.8×10^5	J/kg
Diffusivity	Freon	D	1×10^{-9}	m^2/s
Surface Tension	Mixture	σ	0.027	N/m

*From Marciano et al. (1986).

Table 3. Initial Concentrations

W_{B_0}	ρ_{L_0} (kg/m^3)	m_p (kg)	m_{B_0} (kg)	IEW kg/kmol
0.043977	1,170.775	1,119.288	51.487	669.83
0.084249	1,180.819	1,081.336	99.483	669.83
0.154692	1,198.808	1,013.363	185.445	669.83
0.170813	1,203.003	997.515	205.488	669.83

Table 4. Thermodynamic and Kinetic Data

Parameter	Symbol	Value	Unit
Heat of Reaction*	ΔH_r	1.988×10^8	J/kmol NCO
Chemical Conversion at Gel Point*	x_{gel}	0.4	
Activation Energy for Chemical Reaction**	E	6.276×10^7	J/kmol
Frequency Factor**	A	3×10^8	s^{-1}

*From Marciano et al. (1982).
**From Rojas et al. (1982).

Parameters for Computation

The concentrations of the blowing agent (freon 11) are selected to be the four concentrations for which experimental final foam density values are reported by Rojas et al. (1982). From the composition data given by them, all the initial conditions are calculated considering that the isocyanate and polyol are reacted in stoichiometric proportions. An initial liquid volume of 1 m^3 is taken as basis. The data used are shown in Tables 1 to 3. Table 4 shows the thermodynamic and kinetic data used and Table 5 the values of the parameters used in the model. The initial temperature was taken as 294.1 K. It was assumed that nuclei and bubbles are absent initially.

Numerical Solution

While nucleation is occurring, characteristics are started from some finite points on the time axis and followed in time until gel point ($x = x_{gel} = 0.4$), when the microstructure becomes fixed by gelation of the reaction mixture and simulation is stopped. Equation 26 is integrated along each of these characteristics. Thus, the values of fV_L at a fixed time can be obtained. This represents a discrete version of the bubble-size distribution: (fV_L) vs. l. The accuracy can be improved by starting a large number of characteristics.

The set of ordinary differential equations is solved simultaneously by the fourth-order Runge-Kutta method having the modification due to Gill. The increment in time is automatically

Table 5. Model Parameters

Parameter	Symbol	Value	Unit
Interaction Parameter in Flory-Huggins Theory	χ	0.5	
Frequency Factor in Nucleation Rate Expression	B	8.6×10^{-11}	s^{-1}
Critical Nucleus Size	l_N	0.4×10^{-6}	m

adjusted on the basis of specified error bound. If absolute error is greater than input upper error bound, increment gets halved; if it is less than upper error bound divided by 50, increment gets doubled. Error weights are defined for all dependent variables according to their respective range of values. The typical value of the upper error bound used is 10^{-3} to 10^{-4}.

The calculation procedure is described in detail for the case of diffusion-controlled mass transfer as it is the more complex case. The simulation starts with the integration of the energy balance and the kinetic equations only, with the contribution of blowing agent evaporation term in the energy balance equation set to zero. Liquid-phase vapor pressure P_V is obtained knowing γ_B, W_B, and P^{sat}. The nucleation rate is evaluated only after P_V exceeds 1 atm. ΔC_B would then attain a positive value, indicating the possibility of mass transfer to take place when nucleation starts. The time at which nucleation starts, that is, at which nucleation rate first becomes positive, is marked as cream time. Once nucleation starts, blowing agent begins to evaporate. Now, the evaporation term is allowed to make its contribution in the energy balance equation and in the remaining governing equations, but only as long as ΔC_B remains positive.

The scheme for integration of the characteristic equations is as follows. From the start of nucleation till it stops completely, a new characteristic curve is started at predetermined time intervals. For each of the new characteristic curve, initial conditions (Eq. 50 and righthand side of Eq. 54) are evaluated at the time it starts and stored in an array. The integral on the righthand side of Eq. 51 is continually evaluated by Runge-Kutta-Gill method, starting from $t = 0$. Thus, that integral is available as a function of time. The value of the integral is also stored in an array at each time when a characteristic is started. To get the bubble size at any time t for a particular characteristic curve started at r, the integral on the righthand side of the Eq. 51 between the limits r and t is required. The value of the integral equals its current value minus the value stored at the starting point of that particular characteristic curve. The bubble size is obtained from the integral value at that moment, the initial condition stored for it, and the temperature at that time, using Eq. 51. In a similar manner, the number density function fV_L for a particular characteristic curve is calculated from Eq. 54 using the initial condition: the righthand side of Eq. 54, stored at the starting point of that curve, bubble size calculated as described above for the same characteristic, and the temperature at that moment. Therefore, a pair of values of l and fV_L are obtained from each characteristic curve and thus gives the bubble-size distribution. These values can be numerically integrated to obtain the first moment f_1V_L and from there according to Eq. 48 at each time step.

The method of solution remains unchanged for the case of surface-resistance-controlled mass transfer, the only difference being that the first moment can be evaluated directly as discussed earlier.

Results and Discussion

The only well documented experimental data available in the open literature are due to Rojas et al. (1982). Even these researchers do not give either the average bubble size or its size distribution. The frequency factor B in the nucleation rate

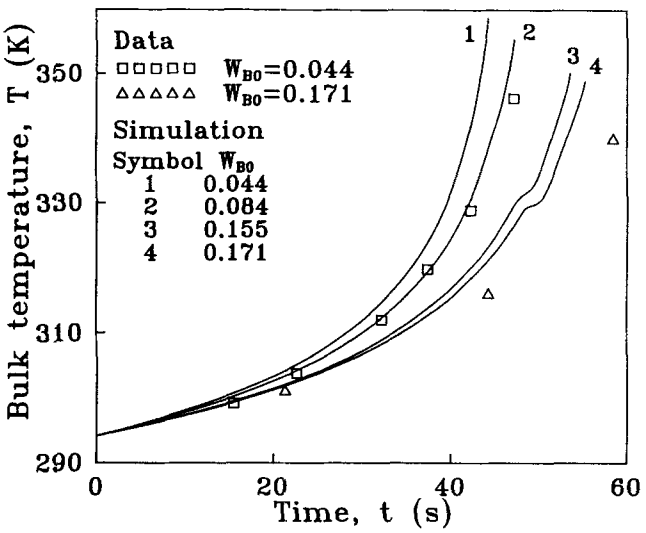

Figure 2. Variation of bulk temperature with time for different initial freon weight fractions.

expression is the only adjustable parameter in the model. The value of B was adjusted to match the experimental bulk foam density data for $W_{B_o} = 0.044$ (Table 3) of Rojas et al. (1982) for the size-dependent bubble growth law. A detailed discussion is presented on the results of the diffusion-controlled growth case. For the case where surface resistance is assumed to control the growth rate, the discussion is focused on the predicted bubble-size distribution only, since this is intended to be a case study aimed at examining the effect of the growth law adopted on the bubble-size distribution.

All graphs presented here are plotted up to rise time, that is, the time of gelation. The parameters used and formulation such as initial concentrations and initial temperature for different models are given in Tables 3-5.

Results of diffusion-controlled mass transfer (constant D)

The variation of temperature with time is presented in Figure 2. The temperature of the system rises with time due to exothermicity of the polymerization reaction. Until cream time is reached, the heat generated is solely used up for heating the system. After that, a part of the heat generated is utilized for blowing agent evaporation. The slope of the curves increases with time, since the system is adiabatic and the reaction is exothermic, not limited by supply of reactants at this stage. The steepness of the curves decreases as we move on to higher initial blowing agent concentrations. The reason is twofold. First, at higher blowing agent concentration, more blowing agent evaporates and hence the heat utilized for evaporation is greater. Secondly, the kinetics of the reaction is slowed down due to the dilution effect caused by the presence of a larger proportion of blowing agent.

A slight flatness is observed in the two curves for the highest blowing agent concentrations. This can be rationalized as follows. As will be discussed shortly, the rise time is less for the formulations with lower W_{B_o} values. Thus, time available for evaporation of blowing agent is less, and correspondingly heat utilized for evaporation is also less. So temperature variation

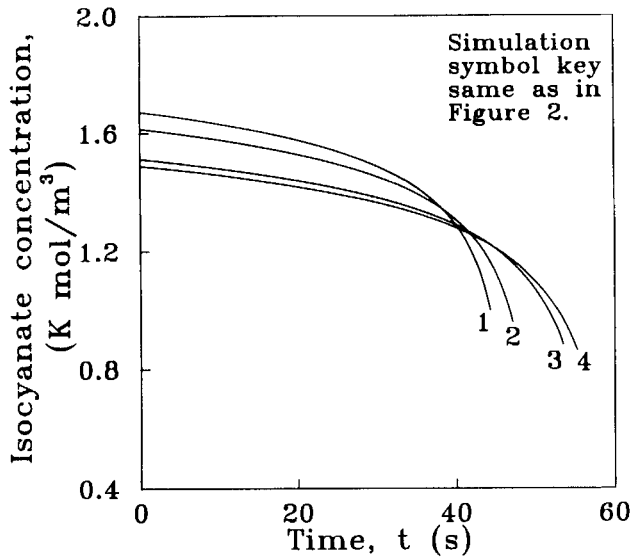

Figure 3. Variation of isocyanate concentration with time for different initial freon weight fractions.

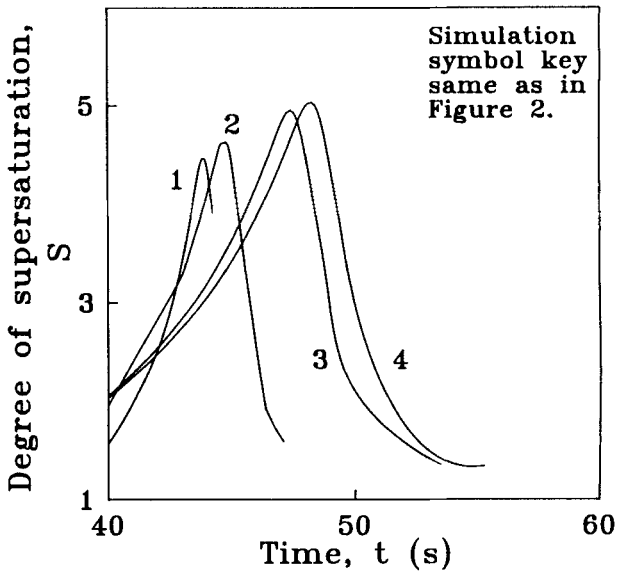

Figure 5. Variation of degree of supersaturation with time for different initial freon weight fractions.

is smooth for lower W_{B_o} values. However, when blowing agent concentration is higher, reaction rates are slower leading to higher rise times and greater amount of evaporation of blowing agent. The rise in temperature is arrested significantly around the period where the blowing agent evaporation rate is high enough to take away a large portion of heat. Temperature values observed by Rojas et al. (1982) are plotted for the lowest and the highest blowing agent concentration for comparison. They are seen to compare well with the simulated values.

Figure 3 shows the fall of Isocyanate concentration with time. Decrease in Isocyanate concentration follows second-order kinetics; as expected, the rate of reaction is lower for higher initial blowing agent concentration. In each curve, the rate of fall of concentration is faster with increasing time and is attributable directly to the rise in temperature.

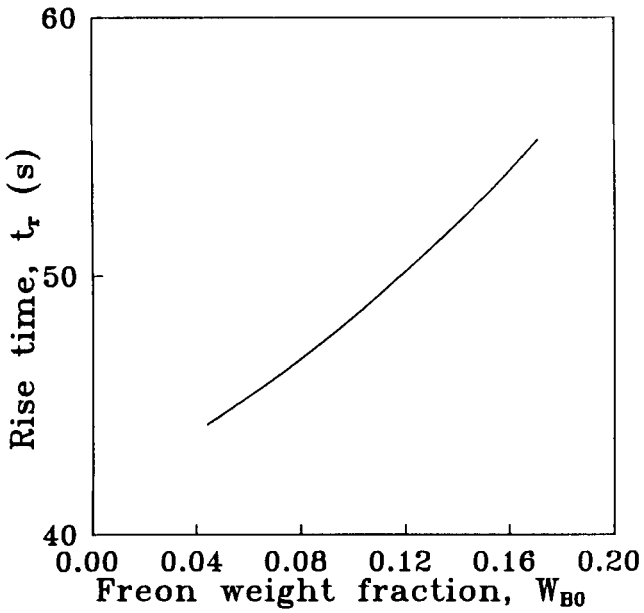

Figure 4. Variation of rise time for different initial freon weight fractions.

Figure 4 shows how rise time, which is the time allowed for the foam to rise or the time taken for attaining gel point, varies with initial freon concentration. Rise time increases with an increase in initial blowing agent concentration and the variation is slightly nonlinear. This is due to slower temperature rise rate for formulations containing more blowing agent initially. As kinetics, and hence time required to attain gel point, is only a function of temperature and initial blowing agent concentration, the nature of the rise time curve is mainly a reflection of slowed-down kinetics in the case of higher W_{B_o}.

The cream time or the time at which bubbles form was found to increase weakly with an increase in initial freon concentration for a fixed initial temperature, because the dilution effect included in the kinetic expression served to retard the temperature rise rate only weakly. This variation is not shown. Thus, the foaming period itself increases with initial blowing agent concentration.

The variation of degree of supersaturation with time is shown in Figure 5. The degree of supersaturation is defined as the ratio of the bulk concentration of freon to that at bubble-liquid interface. The supersaturation increases initially and then falls. As temperature increases with time, the saturation vapor pressure of freon also increases, and hence C_B^* decreases. Freon concentration in the bulk, C_B, remains constant till cream time is reached. Thus, supersaturation can be expected to increase till nucleation begins. Even after nucleation starts, till the nucleation rate becomes significantly large, the number of nuclei present are small. Therefore, the rate of decrease of C_B due to evaporation in the bubble phase is lower than the rate at which C_B^* is falling. Thus, supersaturation increases for a little longer period after nucleation starts. But as more and more nuclei form and grow, the mass-transfer rate increases and blowing agent gets depleted in the liquid phase faster.

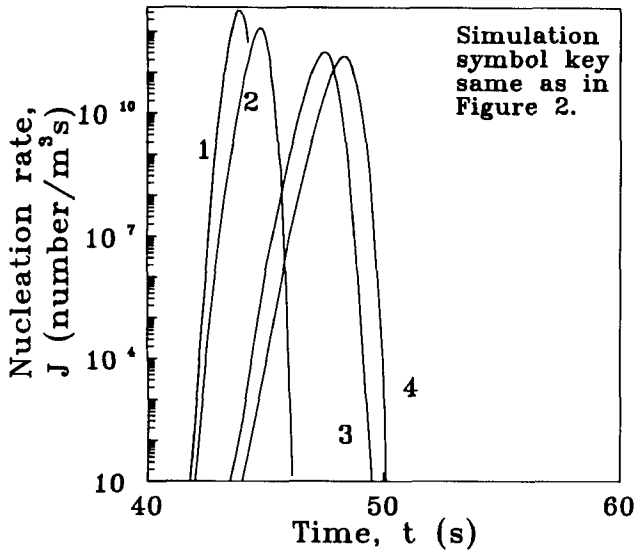

Figure 6. Variation of nucleation rate with time for different initial freon weight fractions.

Thus, in the final stages, the rate of decrease of C_B is greater than that of C_B^*, and supersaturation decreases.

As discussed earlier, the rate of rise of temperature is faster for lower initial freon concentrations. Steeper temperature curves also imply sharper increase in the degree of supersaturation. These features are also observed in Figure 5. As also discussed earlier, the rise times are greater for larger blowing agent concentrations. Thus, the curves become broader with increased blowing agent concentrations.

An interesting point to note here is that for lower initial blowing agent concentrations, nucleation can occur even when gel point is reached. Thus, the rise time is reduced at lower blowing agent concentrations to such an extent that evaporation of blowing agent is not complete before gelation occurs. This indeed depends on the conversion to be achieved to reach

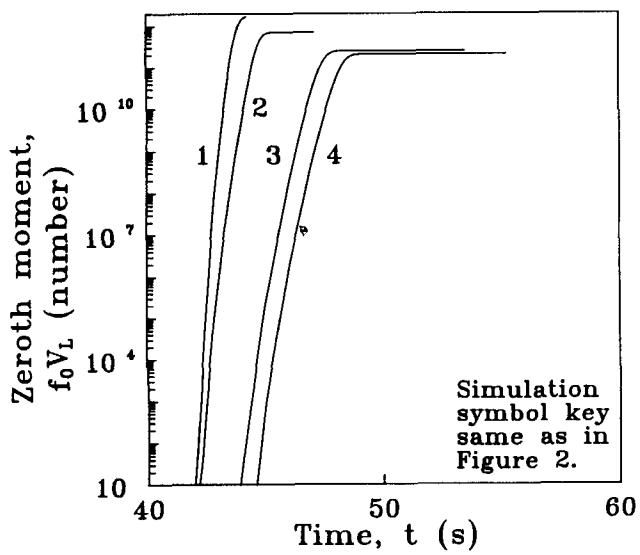

Figure 7. Variation of zeroth moment with time for different initial freon weight fractions.

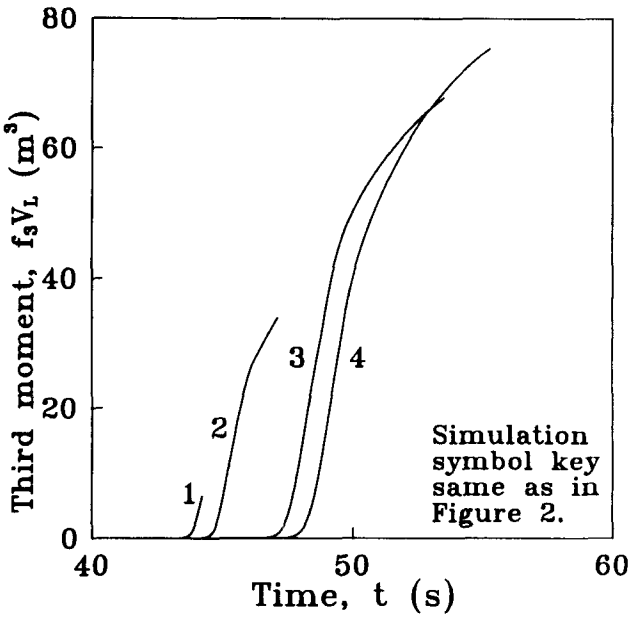

Figure 8. Variation of third moment with time for different initial freon weight fractions.

the gel point. In some material systems, gelation can be achieved at conversions as low as 20%. In these systems, very little vaporization can be expected.

Figure 6 shows the plot of nucleation rate vs. time. Its features are similar to those of the supersaturation vs. time plots and can be explained on exactly the same lines as discussed above. Note that nucleation rates are larger with lower initial blowing agent concentrations. As discussed earlier, an increase in temperature is greater for lower initial blowing agent concentration. Moreover, the supersaturation levels reached are comparable. The increased temperatures thus cause greater nucleation rates.

The zeroth moment of bubble-size distribution, which is equal to the total number of bubbles in the system, is shown as a function of time in Figure 7. It has similar features as the plot of nucleation rate. As discussed earlier, lower blowing agent concentrations lead to greater nucleation rates. Thus, with lower values of W_{B_0}, the total number of bubbles is expected to be higher, as shown in Figure 7. Here, f_0V_L remains constant once nucleation stops, since then the total number of bubbles in the system remains constant. The third moment vs. time is plotted in Figure 8. This does not remain constant after the end of nucleation, as f_0V_L does, but increases with time as the bubble diameter increases due to mass transfer. The first and second moments, not shown here, show similar behavior.

Final foam volume is given by

$$V_f = V_L + \frac{\pi}{6} f_3 V_L$$

is plotted against initial freon concentration in Figure 9. This shows a nonlinear dependence at either end of concentration and a linear increase in the middle. The increasing trend is due to the fact that when initial blowing agent concentration is higher, rise time is longer. As a result, more blowing agent gets evaporated to give a higher final volume. As explained

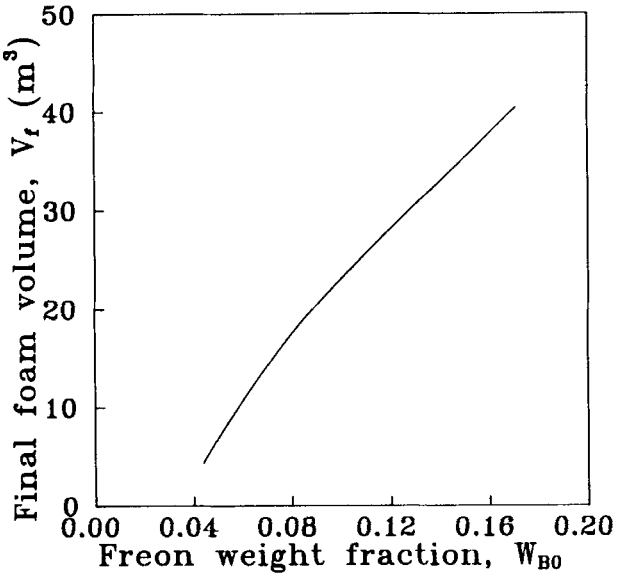

Figure 9. Variation of final foam volume with initial freon weight fraction.

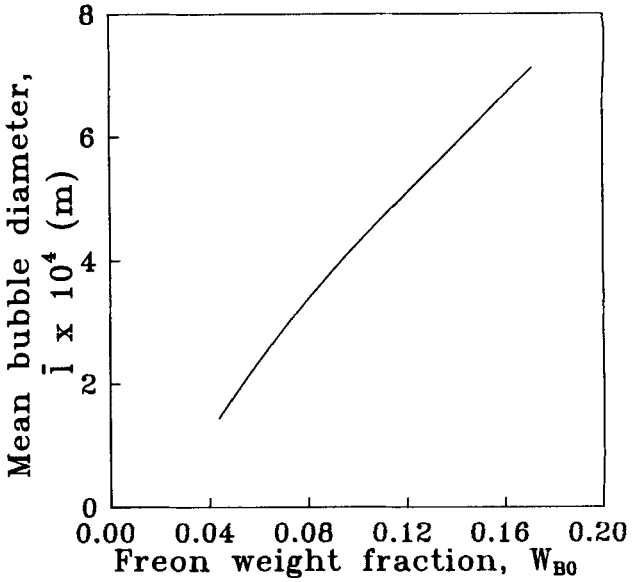

Figure 11. Variation of mean bubble size with initial freon weight fraction.

earlier, the foaming period, that is, the difference between rise time and cream time, increases with an increase in W_{B_0}, almost solely due to the increasing trend of rise time, as cream time does not vary significantly. Thus, the nonlinear trend at low W_{B_0} parallels that of rise time curve. However, at the highest values of initial blowing agent concentration, considerable amount of heat has to go into vaporization of a blowing agent also. This restricts the final foam height achieved. Hence, the final foam volume tends to saturate off at higher blowing agent concentration.

The effect of conversion of NCO groups on the mean bubble diameter is shown in Figure 10. The increase in mean bubble size is faster for higher initial blowing agent due to higher rate of mass transfer as well as due to lower nucleation rates. For W_{B_0} = 0.171, almost all the blowing agent has gone into the vapor phase at fractional conversion x of about 0.3, and the size of the bubbles subsequently increases mainly due to thermal expansion. However, for W_{B_0} = 0.044, gelation occurs even before evaporation of the blowing agent is complete.

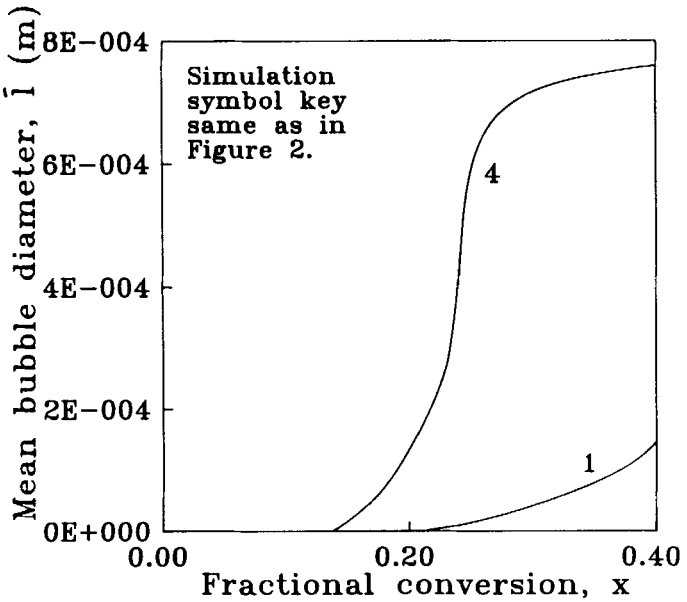

Figure 10. Variation of mean bubble size with fractional conversion of NCO groups for W_{B0} = 0.044 and 0.171.

The final volume fraction of gas phase was in general found to vary from 0.87 to 0.99, when W_{B_0} was varied from 0.044 to 0.171. Such high values of dispersed-phase volume fraction are unlikely to be reached, if the bubbles are spherical and their size distribution is not abnormal. Thus, the morphology of the foam has to change from that of a froth of spherical bubbles to cellular polyhedral structure, when the gas-phase volume fraction becomes very high (for uniform-sized bubbles in FCC packing, this value is 0.74). Beyond this value, the bubbles can no longer be spherical, and the calculation of mass transfer based on spherical bubbles will not yield correct values. It will require a separate treatment (not attempted in this work), since liquid will be present in the form of thin films and plateau borders.

Final bubble-size distribution

Figure 11 shows the variation of mean bubble size obtained as a function of freon weight fraction. Figure 7 shows that the total nuclei present in the system decrease with increasing blowing agent concentration and the effect levels off. Due to an increase in rise time, however, the amount evaporated increases with increased W_{B_0}. Hence, the average bubble size also increases with W_{B_0}.

The final bubble-size distribution at gel point is shown in Figure 12. The growth rate of bubbles is a function of both bubble size and time. Bubble size increases with its age. Therefore, bubbles born at or around cream time contribute to the population of the biggest bubbles. Therefore, there will be no bubble with size greater than that corresponding to those born at cream time, and hence fV_L is zero beyond this size. Thus,

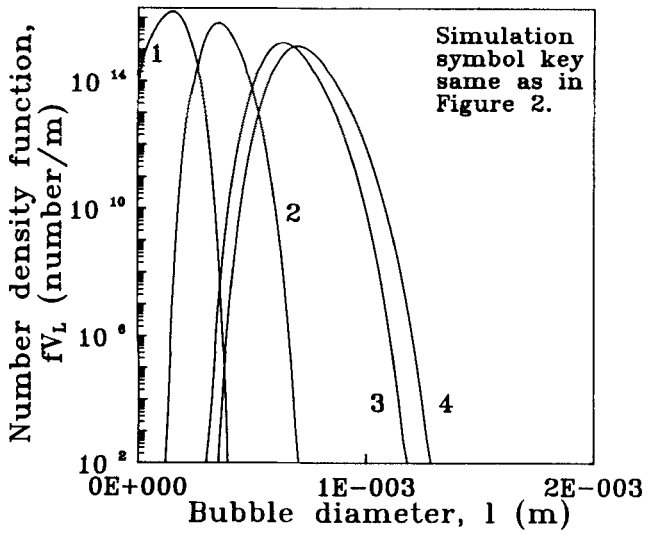

Figure 12. Final bubble-size distribution as a function of initial freon weight fraction (constant *D*).

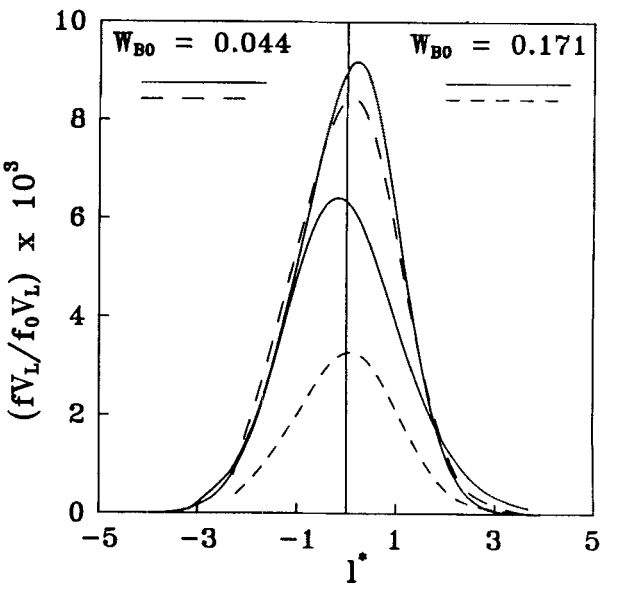

Figure 13. Variation of bubble-size distribution with time for W_{B0} = 0.044 and 0.171 (constant *D*).

if supersaturation buildup is rapid as in the case of W_{B_0} = 0.044, there will be a sharp fall in fV_L at the larger size end. Bubbles born at an intermediate time constitute the main population around the mean size. The smaller bubbles are obtained from those that come from the nuclei formed near the end of nucleation period, as they had lesser time to grow before gelation occurred. Here, we see a gradual decrease of fV_L for higher blowing agent concentrations since nucleation stopped before gelation occurred. In contrast, fV_L is still fairly high for 0.044, since even at gel point nucleation was still possible. An important property of the distribution is its breadth. A measure of breadth is the difference between the sizes of the largest and the smallest bubbles. It is evident that the breadth of the distribution will increase with the difference between the time available for the very first-born and the very last-born bubbles to grow. Thus, increased rise times and nucleating periods tend to broaden the distribution. However, the growth rates of all the bubbles are not the same. Bigger bubbles grow at a lower rate than smaller ones as the growth rate due to diffusional mass transfer shows an inverse relationship with the bubble size. Thus, as time progresses, this growth rate law tends to decrease the breadth of the distribution. The latter effect is complicated by the variation of driving force with time. Thus, ΔC_B increases with time initially and decreases subsequently. Thus, bubbles born during the period when ΔC_B increases with time will grow faster than those born earlier. This has an effect of narrowing the distribution. Exactly the opposite is true with bubbles born during the period when ΔC_B decreases with time. The final breadth of the distribution is a result of the complex interplay of these effects.

To compare the bubble-size distributions obtained for different W_{B_0} values, a normalized length scale is chosen which is defined as:

$$l^* = \frac{(l - \bar{l})}{\mathrm{Var}(l)}$$

If fV_L, normalized by f_0V_L, is plotted against l^*, it is possible to compare bubble-size distributions having different mean and variance values. Figure 13 shows the transient (dashed lines) and final bubble-size distribution (solid lines) for the two extreme W_{B_0} values. In general, the bubble-size distributions are broadening with time, the final distribution being broader for higher W_{B_0}. Evidently, the dominant factor that determines the breadth of distribution is the difference in the time periods of growth of the bubbles born at cream time and gel time.

Foam density

Figure 14 shows the bulk density obtained at gel point as a function of formulation. The bulk density can be evaluated using Eq. 27. There is an initial sharp decrease in bulk density that levels off at higher initial freon concentrations. The nu-

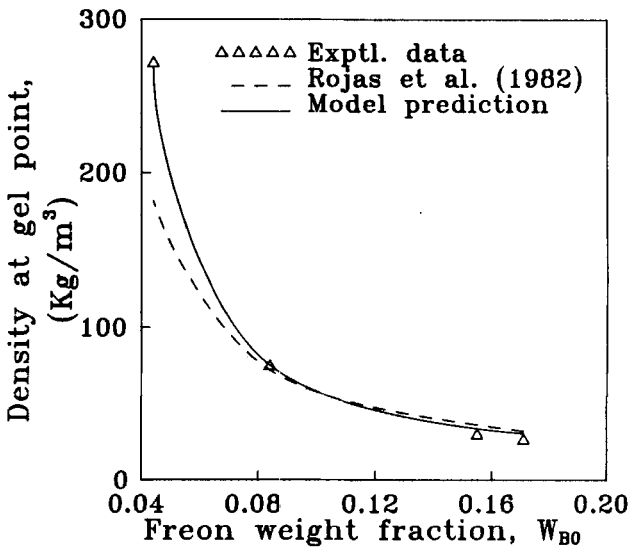

Figure 14. Variation of final foam density with initial freon weight fraction (constant *D*).

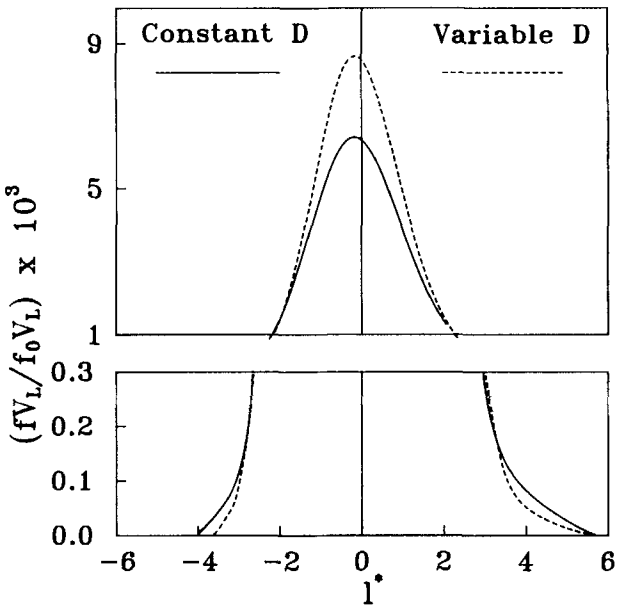

Figure 15. Final bubble-size distribution for $W_{B0} = 0.171$: variable vs. constant D models.

cleation rates in Figure 6 show that for lower blowing agent concentrations, gelation occurred around the time when the nucleation rate was at its peak. Hence, the system contained a large number of nuclei that had not had enough time to grow before gelation sets in. Thus, incomplete evaporation of blowing agent resulted in higher final foam density. But, when the initial blowing agent concentration is higher due to longer rise time, the nucleation was complete and bubbles had time to grow. Therefore, in this case, blowing agent evaporation is more or less complete and there is hardly any blowing agent left in the liquid phase to evaporate ahead of rise time. Then, the bubbles expand slowly due to an increase in temperature and in the presence of low mass-transfer rate. So, the rapid decrease and flattening of the density curve are essentially reflecting the variation of the amount of the blowing agent that got evaporated.

Rojas et al. (1982) have reported experimental density values as well as values predicted by their model as a function of four initial blowing agent concentrations. These values are compared with the predicted density values of this model. Even though at higher freon concentrations the density values are almost the same, at lower concentrations this model predicts density values much closer to the experimental values, compared to the simulated values by Rojas et al. (1982), with the latter showing an appreciable deviation in that region.

One noteworthy point is that for the lowest initial blowing agent concentration, the final foam density value showed maximum sensitivity with respect to the adjustable parameter B appearing in nucleation rate expression. For high W_{B_0}, density values were quite insensitive to B.

Results of diffusion-controlled mass transfer (variable D).

For this model, the computations revealed features qualitatively similar to those presented so far. The growth rate of bubbles is a function of time and size in this case also. However, in this case, the mass-transfer coefficient for a bubble decreases with time, because not only its size is increasing but also the diffusion coefficient is decreasing. Hence, the growth rate of bubbles of any given size is smaller at every instant in comparison with the previous case. Thus, the main difference lies in the breadth of the distribution.

The final bubble-size distribution obtained in this case is presented in Figure 15. The final bubble-size distribution obtained with constant D is also presented for easy comparison. Features similar to those described in Figure 13 are present here as well. However, the distribution obtained with the variable diffusion coefficient is marginally narrowed. As discussed earlier, the breadth of the distribution is proportional to the difference in time period of growth of the first- and the last-born bubbles, and their growth rates. The former is influenced mostly by the kinetics of the process that is relatively unaffected by the growth model assumed. Thus, the difference between the constant and variable diffusion coefficient models is dictated entirely by the difference in the growth rate of the first and last bubbles. The difference will be smaller, and hence the breadth of the distribution will also be smaller for the model that gives smaller growth rates. Hence, it is found that the distribution is narrower for the variable diffusion coefficient model than for the constant diffusion coefficient model.

Influence of heterogeneous nucleation

It is now pertinent to discuss the effects of other types of nucleation. If extraneous solid particles are present in the system, heterogeneous nucleation will occur. The activation energy for this type of nucleation is lower, and thus heterogeneous nucleation can be expected to occur at lower supersaturation and hence at an earlier stage of polymerization than homogeneous nucleation. Thus, the time available for growth of bubbles is greater with heterogeneous nucleation. Hence, at lower blowing agent concentrations where gelation occurred before all the blowing agent has evaporated, we can expect mean bubble size to be larger if heterogeneous nucleation occurs. The rate of heterogeneous nucleation depends on the number of sites available for nucleation. If sufficient sites are available, the rate of heterogeneous nucleation is greater than the rate of homogeneous nucleation, and this has the effect of creating larger number of nuclei in a comparable time interval. Large number of nuclei reduce the supersaturation quickly, thereby suppressing further nucleation. The net result is that the nucleation is confined to a shorter time interval. Consequently, the bubble-size distribution is expected to be narrower. The same comments apply to the case when a sufficient number of small air bubbles are introduced in the reaction mixture before injection into the mold.

The above discussion assumes that a large number of sources for formation of heterogeneous nuclei are available. If such is not the case, some homogeneous nucleation can also occur simultaneously and the results will be appropriately altered.

Results of surface-resistance-controlled mass transfer

In this model we assume mass transfer to be controlled entirely by constant surface resistance. The rationale for this model has been already discussed. In this model, the growth rate is still weakly dependent on bubble size, but only through the thermal expansion term. It is also a function of time as

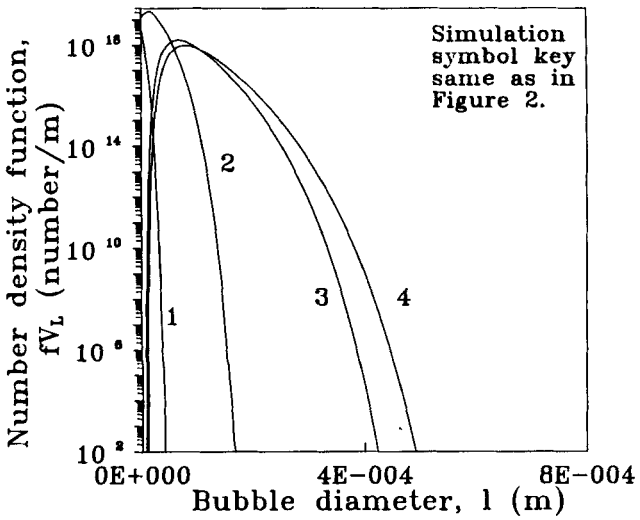

Figure 16. Final bubble-size distribution as a function of initial freon weight fraction (surface resistance-controlled growth).

before. A typical value of 10^{-6} m/s is chosen for k_S, such that the mass-transfer resistance offered equals that in the diffusional mass transfer for bubbles around the mean size.

Figure 16 shows the plot of number density function fV_L vs. bubble diameter l for different initial blowing agent concentrations. Here also distribution of the bubble size is age-dependent for the reasons discussed earlier. Because of a very low and constant mass-transfer coefficient, the growth rate is lower than in the previously described situations. Therefore, a sharper distribution is obtained as expected. Further, the number of bubbles nucleated is greater here since the slower growth rates do not permit quick lowering of supersaturation. In fact, this effect is so important that for $W_{B_o} = 0.044$, even at gel time, the nucleation rate is still high.

Normalized fV_L is plotted against l^* in Figure 17. The bubble-size distributions for $W_{B_o} = 0.044$ show a monotonic decrease. This is entirely due to the fact that supersaturation is increasing even at gel time, and thus nucleation rate is still large. The regular bell-shaped size distribution is reached only when supersaturation starts falling before gel time is reached. For higher W_{B_o}, however, the rise time being higher, supersaturation eventually falls down giving a final bell-shaped distribution.

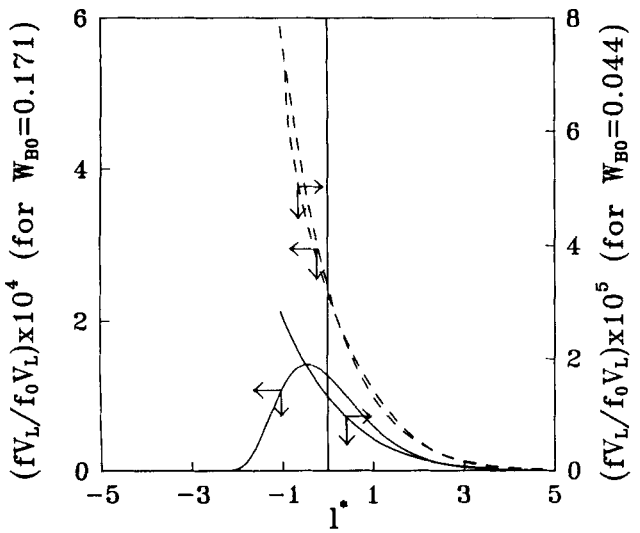

Figure 17. Variation of bubble-size distribution with time for $W_{B0} = 0.044$ and 0.171 (surface resistance-controlled growth).

The cross-comparison of bubble-size distributions obtained form surface-resistance-controlled growth law and that from diffusion-controlled growth rate law shows the distribution is narrower for the former. It was observed that the nucleating period for both cases was found to be nearly the same. Thus, the narrowing-down has to be attributed to the history of the driving force for growth. This can be explained as follows. Due to the higher mass-transfer resistance, the evaporation rate of the blowing agent is less, and thus the driving force for growth and nucleation rate is higher than in the diffusional mass-transfer case. Thus, bubbles seem to experience more uniform conditions of growth. A larger number of nuclei growing under higher mass-transfer resistance can then be expected to generate a bubble-size distribution that constitutes smaller bubbles and is narrower.

The approach adopted in getting bubble-size distribution for this particular system can be applied in the foaming systems where the blowing agent is generated by another reaction, for example, water-blown RIM. This involves the inclusion of the additional reaction kinetics term in the equations for balance of isocyanate. Further, mass balance for CO_2 generated can be used to calculate the supersaturation, nucleation rates, and finally mass-transfer rates. A system containing more than one blowing agent can also be simulated following the approach given here. It appears that such a practice is aimed at generating bimodal bubble-size distribution. In this case, the second blowing agent can evaporate into the bubbles already present, and this will tend to suppress nucleation of the second blowing agent. This has to be incorporated in the model.

Conclusions

A model of solvent-blown free rise foams generated by the RIM process has been developed. Usual energy and mass balance have been coupled to the bubble-size distribution through the evaporation rate of solvent. A population balance has been used to generate the bubble-size distribution. The bubble-size distribution was found to become broader as the initial weight fraction of the blowing agent was increased. If the mass-transfer resistance to evaporation can be increased, the bubble-size distribution tends to become narrower.

Acknowledgment

We acknowledge the Department of Science and Technology, New Delhi, for partial support through project II - 3 (18)/87.

Notation

A = frequency factor for chemical kinetics, s^{-1}
$AntA$ = Antoine constant
$AntB$ = Antoine constant
$AntC$ = Antoine constant
B = frequency factor of gas bubbles joining the nucleus, s^{-1}

C_B = concentration of blowing agent in bulk liquid, kmol/m^3
C_B^* = concentration of blowing agent at bubble-liquid interface, kmol/m^3
ΔC_B = $(C_B - C_B^*)$, kmol/m^3
c_{p_B} = specific heat of blowing agent in the liquid phase, J/kg·K
c_{p_g} = specific heat of blowing agent in the gas phase, J/kg·K
c_{p_p} = specific heat of polymer and prepolymer, J/kg·K
D = diffusion coefficient, m^2/s
E = activation energy for chemical kinetics, J/kmol
$f(l)$ = number density function of bubbles in the size range l to $l + dl$, m^{-4}
$f_n V_L$ = nth moment of bubble size distribution, m^n
ΔF^* = minimum free energy change for the formation of critical nucleus (classical nucleation theory), J/kmol
ΔF_p^* = net free energy change for the formation of critical nucleus, J/kmol
ΔF_S = free energy change for the formation of critical nucleus due to supersaturation, J/kmol
ΔF_I = free energy change for the formation of critical nucleus due to nonideality, J/kmol
G = growth rate of bubbles, m/s
ΔH_r = heat of reaction, J/kmol
IEW = isocyanate equivalent weight, expressed in mass of polymer per kmol of isocyanate, kg/kmol
J = nucleation rate, no./m^3·s
k = Boltzmann constant, J/molecule·K
k_D = diffusional mass-transfer coefficient, m/s
k_m = mass-transfer coefficient, m/s
k_S = surface resistance offered by surfactant, m/s
l = bubble diameter, m
l_N = critical nucleus size, m
l^* = normalized bubble size
m_B = mass of blowing agent in liquid phase, kg
m_p = mass of polymer and/or prepolymers, kg
M = number of molecules of blowing agent/unit volume of polymer solution, no./m^3
M_B = molecular weight of blowing agent, kg/kmol
n = total number of blowing agent molecules in a critical nucleus
$N(l)$ = mass-transfer rate into bubble of size l, kmol/s
P = pressure, N/m^2
P_L = pressure in the liquid phase, N/m^2
P^{sat} = saturation vapor pressure of the blowing agent, N/m^2
P_V = vapor pressure of the liquid phase, N/m^2
r = point marking the beginning of a characteristic
R = gas law constant, J/kmol·K
S = degree of supersaturation
t = time, s
t_c = cream time, s
t_{gel} = gel time, s
t_r = rise time, s
T = temperature, K
T^* = boiling point of the solution at atmospheric pressure, K
V = volume of the foam at any time, m^3
V_f = final volume of the foam, m^3
V_L = volume of the liquid phase, m^3
W_B = weight fraction of blowing agent
W_B^* = weight fraction of blowing agent at gas-liquid interface
x = fractional conversion of reactive species
x_{gel} = chemical conversion to gelation
Z = distance along a characteristic curve

Greek letters

γ_B = liquid phase activity coefficient
λ = latent heat of vaporization, J/kg
ρ_{all} = overall foam density at gel point, kg/m^3
ρ_B = density of the blowing agent, kg/m^3
ρ_L = density of the liquid phase, kg/m^3
ρ_p = density of polymer and prepolymer, kg/m^3
σ = surface tension, N/m
χ = interaction parameter
Φ = volume fraction of polymer

Subscripts

o = initial condition
B = blowing agent
g = gas
L = liquid phase
p = polymer, prepolymer

Literature Cited

Amon, M., and C. D. Denson, "A Study of the Dynamics of Foam Growth: Analysis of the Growth of Closely Spaced Spherical Bubbles," *Polym. Eng. Sci.*, **24**, 1026 (1984).

Amon, M., and C. D. Denson, "A Study of the Dynamics of Foam Growth: Simplified Analysis and Experimental Results for Bulk Density in Structural Foam Molding," *Polym. Eng. Sci.*, **26**, 225 (1986).

Campbell, G. A., "Integral-skin Foam: a Mechanism for Skin Formation," *J. Appl. Polym. Sci.*, **16**, 1735 (1972a).

Campbell, G. A., "Polyurethane Foam Process Development: a Systems Engineering Approach," *J. Appl. Polym. Sci.*, **16**, 1387 (1972b).

Han, J. H., and C. D. Han, "Bubble Nucleation in Polymeric Liquids: I. Bubble Nucleation in Concentrated Polymer Solutions," *Polym. Eng. Sci.*, **28**, 711 (1990a).

Han, J. H., and C. D. Han, "Bubble Nucleation in Polymeric Liquids: II. Theoretical Considerations," *Polym. Eng. Sci.*, **28**, 743 (1990b).

Lipshitz, S. D., and C. W. Macosko, "Kinetics and Energetics of a Fast Polyurethane Cure," *J. Appl. Polym. Sci.*, **21**, 2029 (1977).

Marciano, J. H., M. M. Reboredo, A. J. Rojas, and R. J. J. Williams, "Integral-skin Polyurethane Foams," *Polym. Eng. Sci.*, **26**, 717 (1986).

Marciano, J. H., A. J. Rojas, and R. J. J. Williams, "Curing Kinetics of a Rigid Polyurethane Foam Formulation," *Polym.*, **23**, 1489 (1982).

Rojas, A. J., J. H. Marciano, and R. J. J. Williams, "Rigid Polyurethane Foams: a Model of the Foaming Process," *Polym. Eng. Sci.*, **22**, 840 (1982).

Shutov, F. A., "Foamed Polymers: Cellular Structure and Properties," *Adv. in Polym. Sci.*, **51**, 155 (1983).

Tighe, S. C., and L. T. Manzione, "Simulation of Foaming in Reaction Injection Molding," *Polym. Eng. Sci.*, **28**, 949 (1988).

Yokono, H., S. Tsuzuku, Y. Hira, M. Gotoh, and Y. Miyano, "Simulation of Foaming Process of Polyurethane Integral-skin Foams," *Polym. Eng. Sci.*, **25**, 958 (1986).

Manuscript received Dec. 30, 1991, and revision received Apr. 28, 1992.